InGaAs Infrared Detectors+

J. KANIEWSKI,*[1] J. PIOTROWSKI[2]

[1] Institute of Electron Technology, Warsaw, Poland
[2] Vigo System, Warsaw, Poland

Recent developments in the design and technology of InGaAs infrared detectors are reviewed. Due to advances in molecular beam epitaxy and metalorganic chemical vapour deposition it became possible to grow strained and relaxed InGaAs layers on different substrates. It enabled for significant extension of spectral range of InGaAs detectors.

1. Introduction

The $In_xGa_{1-x}As$ ternary alloys cover a wide range of lattice constants between GaAs (x = 0: a = 0.5653 nm, E_g =1.43 eV) and InAs (x = 1: a = 0.6058 nm, E_g = 0.35 eV). Except the alloy with composition $In_{0.53}Ga_{0.47}As$, which is lattice-matched to InP, all other $In_xGa_{1-x}As$ compounds grown on GaAs or InP substrates are mismatched materials. Therefore, instead of one ternary compound, we have to deal with three different structures, relaxed and compressively or tensilely strained ones. The properties of these structures differ considerably.

$In_xGa_{1-x}As$ is a direct-gap semiconductor for any value of x between 0 and 1. $In_{0.53}Ga_{0.47}As$ (E_g = 0.74 eV at T = 300 K), lattice – matched to InP, is widely used due to high mobility, high velocity of electrons and large intervalley separation in the conduction band. For these reasons field-effect transistors made of this material have record static, frequency, and noise characteristics. Moreover, the bandgap of $In_{0.53}Ga_{0.47}As$ corresponds to a spectral range where both the losses and dispersion of optical fibres are very low. Therefore, $In_{0.53}Ga_{0.47}As$ is also used to fabricate sources, modulators and detectors of near infrared radiation.

It is very rare for a semiconductor to be applied both in electronics and optoelectronics. For this unique reason $In_xGa_{1-x}As$, as well as its heterostructures, are used in optoelectronic integrated circuits.

The area of applications of strained $In_xGa_{1-x}As$ has been growing fast for the last few years. Relaxed layers are used in bandgap engineering, whereas strained material is used in engineering of both bandgap and band structure. Due to the development of such modern techniques as MBE (Molecular Beam Epitaxy) or MOCVD (Metalorganic Chemical Vapour Deposition) very thin films with thicknesses below 10 nm may be fabricated. Because of that $In_xGa_{1-x}As$ epitaxial layers grown nowadays may have lattice constants considerably different from those of the substrate. These techniques contributed also to the crea-

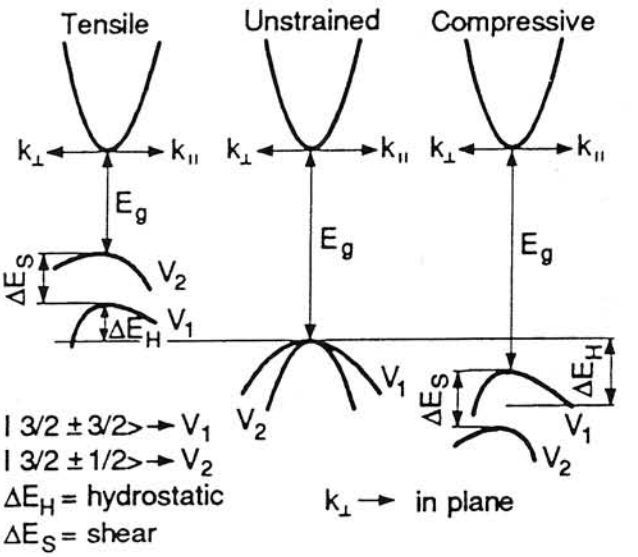

Fig. 1. Changes of $In_xGa_{1-x}As$ band structure under the influence of compressive and tensile strain [1].

*corresponding author: Janusz Kaniewski, Institute of Electron Technology, 32/46 Al. Lotników, 02-668 Warsaw, Poland;

+ Presented at the 12th School of Optoelectronics: Photovoltaics – Solar Cells and Infrared Detectors, Kazimierz Dolny. May 22-24, 1997.

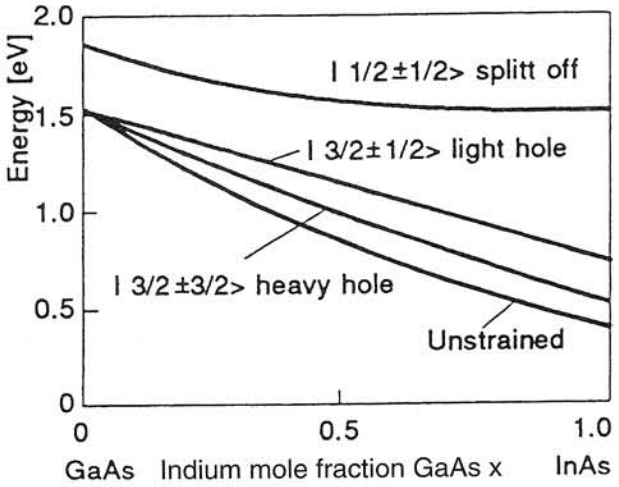

Fig. 2. Bandgap in $In_xGa_{1-x}As$ grown on (001) GaAs. Compressive strain increases the energy distance between the bands of heavy and light holes and the conduction band [2].

tion of a new group of quantum detectors of radiation – QWIPs (Quantum – Well Infrared Detectors). Devices of this type contain $In_xGa_{1-x}As$ quantum wells and may detect mid and far infrared radiation.

2. Strain versus band structure of $In_xGa_{1-x}As$ layers

If $In_xGa_{1-x}As$ layers (regardless of the value of x) grown on (001) GaAs are not relaxed through generation of misfit dislocations, they are subjected to biaxial in-plane compression with simultaneous extension along the [001] direction of growth. $In_xGa_{1-x}As$ (x 0.53) grown on InP is exposed to a similar strain. On the other hand, $In_xGa_{1-x}As$ (x 0.53) grown on (001) InP

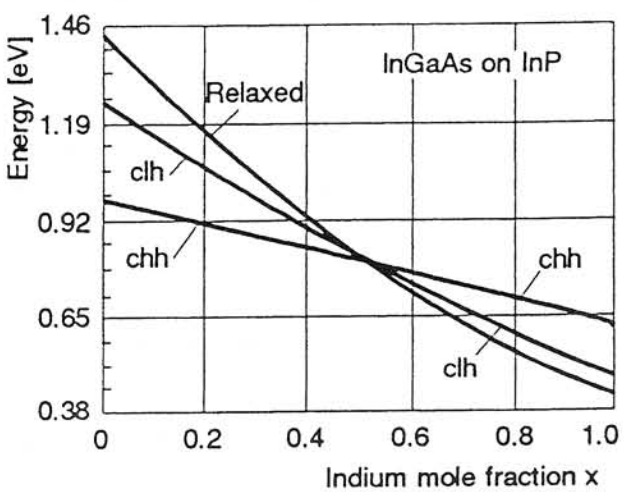

Fig, 3. Influence of strain on energy distances in $In_xGa_{1-x}As$ grown on (001) InP [3].

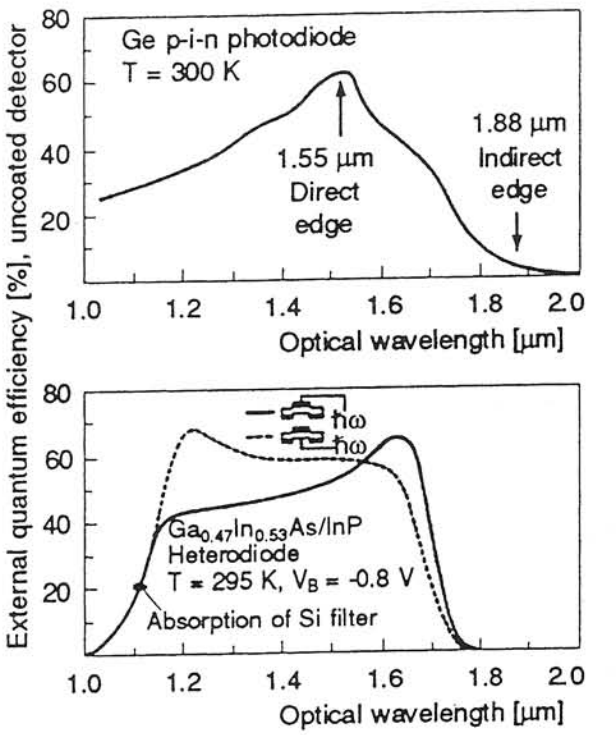

Fig. 4. Spectral response of: a) Ge photodiode at T = 295 K. Two different slopes are observed at 1.8 μm and 1.55 μm. These are the result of indirect gap absorption and direct gap absorption, respectively. b) $In_{0.53}Ga_{0.47}As$ photodiode at 295 K. A fast increase of response in the vicinity of 1.6 μm is caused by direct gap absorption.

is subjected to in-plane tensile strain with simultaneous out-of-plane compression. Qualitative changes of the band structure due to the strain are schematically shown in Fig.1. Strain eliminates the degeneracy of the heavy-hole band V_1 and the light-hole band V_2. Simultaneously, tensile strain causes V_2 band (nominally the light-hole band) to move above V_1 one . Nevertheless, as can be seen from the curvature of the bands, the values of effective masses of light and heavy holes are strongly dependent on the crystallographic direction. The relation between lattice constants indicates that $In_xGa_{1-x}As$ grown on GaAs is always subjected to compressive strain, whereas the same compound grown on InP may be exposed either to tensile or compressive strain, depending on the value of x. Quantitative changes of the energy bandgap due to strain in $In_xGa_{1-x}As$ layers grown on GaAs and InP are shown in Figs. 2 and 3, respectively.

It is worth noticing that considerations concerning strain correspond to relatively thin layers, whose thickness is below the so-called critical thickness t_c. The value of t_c strongly depends on the stoichiometry of both layer and substrate, as well as on the temperature of growth. It is usually lower than 10 nm. Nevertheless,

in the case of profiled substrates strained $In_{0.11}Ga_{0.89}As$ layers with a thickness of 150 nm and $In_{0.15}Ga_{0.85}As$ layers with a thickness of 90 nm were fabricated on GaAs [4].

3. PIN photodiodes

The most important parameters of a photodiode are spectral response, quantum efficiency, speed of operation, capacitance, dark current and reliability. $In_xGa_{1-x}As$ is a material which enables detectors with optimal parameters in all the above categories to be fabricated. In the (1 ÷ 2) μm spectral range germanium is the only competitor to $In_xGa_{1-x}As$ diodes. Ge detectors do not, however, match the speed of operation and noise characteristics of $In_xGa_{1-x}As$ ones. Spectral characteristics of both detectors are shown in Fig. 4.

The spectral response of $In_xGa_{1-x}As$ photodiodes, similarly to other semiconductors, is determined by the bandgap. The spectral response for above bandgap photons is determined by the absorption coefficient α. In $In_xGa_{1-x}As$ the value of α reaches 10^4 cm^{-1} for energies several kT higher than the bandgap. In this spectral range all photons are absorbed within the distance of several μm from the surface. On the other hand, for $h\nu \cong 1$ eV the absorption coefficient $\alpha \cong 10^5$ cm^{-1} and the majority of photons are absorbed very close to the surface. Such strong changes of α lead to a decrease of the photocurrent of minority carriers reaching the p-n junction for shorter wavelengths (< 1.5 μm) due to surface recombination (Fig. 4).

The maximum quantum efficiency for $In_xGa_{1-x}As$ photodiodes is approximately 75%, which is determined by optical reflection at the air/semiconductor

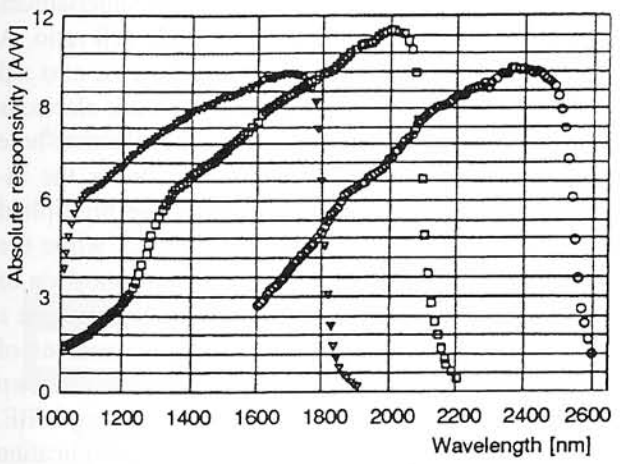

Fig. 5. Spectral characteristics of $In_xGa_{1-x}As$ photodiodes ($x \geq 0.53$) grown on InP (lattice mismatched) in EPITAXX Inc. by means of hydride vapour phase epitaxy.

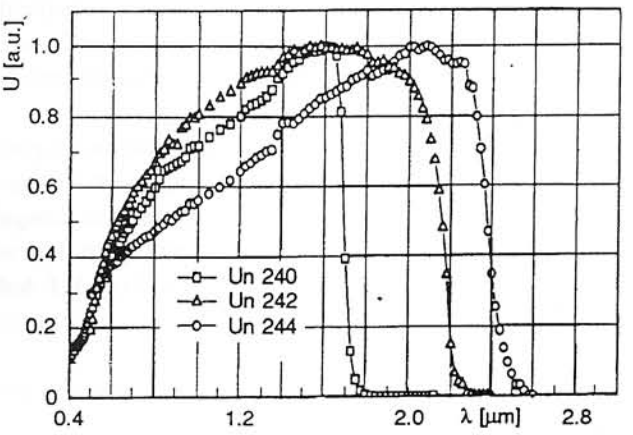

Fig. 6. Spectral characteristics of $In_xGa_{1-x}As$ photodiodes ($x \geq 0.53$) grown on GaAs (lattice mismatched) in IET by means of MBE.

interface. Antireflection coatings, however, increase quantum efficiency to nearly 100% [5]. Increasing the contents of InAs above 53% enables the absorption edge to be moved above approximately 3.5 μm. Therefore, important spectral ranges, such as the short-wave window (2 ÷ 2.5) μm and the short-wave part of the (3 ÷ 5) μm window in which atmosphere is transparent are partially covered. This requires, however, fabrication of relaxed layers which are lattice mismatched to the substrate. At present there are two methods of fabrication of such layers. In the first method a thick layer (≅ 20 μm) is grown on InP with the composition graded linearly. This layer is followed by a highly doped layer (≅ 2 μm). Finally, the appropriate detector structure is grown [6]. In the second method the thick layer is replaced by several thin layers (< 0.2 μm) with composition changed abruptly. The quality of the interfaces on which misfit dislocations are generated is in this case of great importance. An important advantage of the second method is the fact that $In_xGa_{1-x}As$ ($x > 0.53$) may be grown also on GaAs, a substrate with a considerably different lattice constant. A comparison of spectral characteristics of ternary compounds fabricated using the two methods is shown in Figs. 5 and 6. Recently, Wojtczuk et al. [7] have grown structures of $In_{0.72}Ga_{0.28}As$ on InP using abrupt composition changes by means of MOCVD.

Photodiodes with extended spectral range (λ < 2.6 μm) have a relatively low dark current (1.1 μA at -5 V), detectivity $D^* \geq 1.5 \times 10^{11}$ $cmHz^{1/2}/W$ and low capacitance 6 pF (0V) and 2 pF (-1V). The parameters of these photodiodes are similar to the typical values encountered in widely used $In_{0.53}Ga_{0.47}As$/InP detectors (λ < 1.7 μm). Due to considerable homogeneity of

the layers and reproducibility of the processes, typical of III-V compounds, 64 × 1 [7], 512 × 1 and 1024 × 1 [8] linear arrays and two-dimensional detector arrays with $\lambda < 2.6$ μm may be produced.

Fabrication of epitaxial layers on silicon is particularly interesting, since it creates prospects for integration of detector technology with silicon image processors. Long-time research on epitaxy of layers which are mismatched material, conducted in MIT, led to fabrication of $In_xGa_{1-x}As$ linear arrays ($\lambda < 2.6$ μm) on profiled Si substrate [9].

The parameters of detectors may be substantially improved through the use of monolithic optical immersion. The transparency of the substrate makes it possible to fabricate lenses directly in the substrate, similarly to $Hg_{1-x}Cd_xTe$ layers on CdTe [10]. Due to high refractory indices of GaAs and Si (≅ 3.4) optical hyperimmersion leads to a reduction of dark current and capacitance by more than two orders of magnitude when compared to a conventional device with the same photosensitive area.

4. Avalanche photodiodes

The value of the noise current caused by avalanche multiplication of carriers is one of the most important parameters of avalanche photodiodes. Due to a relatively low value of this current avalanche photodiodes are competitive with respect to other types of photodiodes, such as PIN photodiodes with a low-noise amplifier. High difference between ionization coefficients of electrons and holes and avoiding of the carriers with lower ionization coefficient from participating in the avalanche multiplication process are required in order to achieve low current of avalanche noise. The fulfilment of the first condition depends on the properties of the material from which the multiplication region is made. While in Si the difference between electron (α) and hole (β) ionization coefficients is so high that α/β ratio reaches approximately 100, it is much lower in other semiconductors (germanium, III-V compounds). Therefore, in silicon avalanche photodiodes for the density of noise current of 1 pA/Hz $^{1/2}$ the gain is usually above 100.

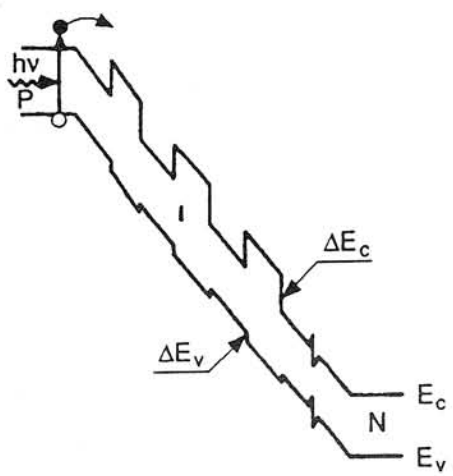

Fig. 7. Band diagram of a superlattice biased so that avalanche multiplication is possible.

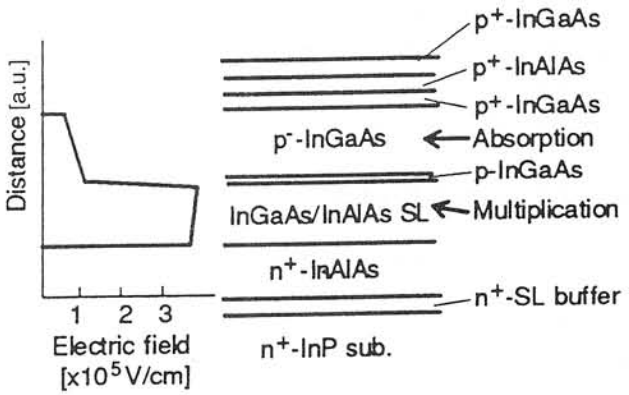

Fig. 8. The structure and distribution of electric field in an SAM p-$In_xGa_{1-x}As$ /superlattice $In_xGa_{1-x}As$ /InAlAs photodiode [12].

In order to meet the second requirement in modern avalanche photodiodes, whether made of silicon or other semiconductors, the region of avalanche multiplication is separated from the region of absorption of photons (SAM APD – Separate Absorption and Multiplication Avalanche Photodiodes). In this way only those carriers whose ionization coefficient is big enough are capable of reaching the multiplication region. Capasso [11] suggested the use of superlattices for carrier multiplication to improve the α/β ratio. A band diagram of such a superlattice in the case of $\alpha > \beta$ is shown in Fig. 7. After reaching the well, electrons cause impact ionization and generate electron-hole pairs. Due to the band configuration under the influence of the applied bias electrons are multiplied by consecutive stages of the superlattice, while the slope of the valence band prevents multiplication of holes. This idea was used in practice to fabricate a p- $In_xGa_{1-x}As$/InP structure with separate regions of absorption and multiplication. The structure is shown in Fig. 8 [12]. The structure, fabricated using MBE, had quantum efficiency of 73% at the multiplication factor of unity. The maximum multiplication factor was, however, relatively low and was equal to 10 at 3 GHz.

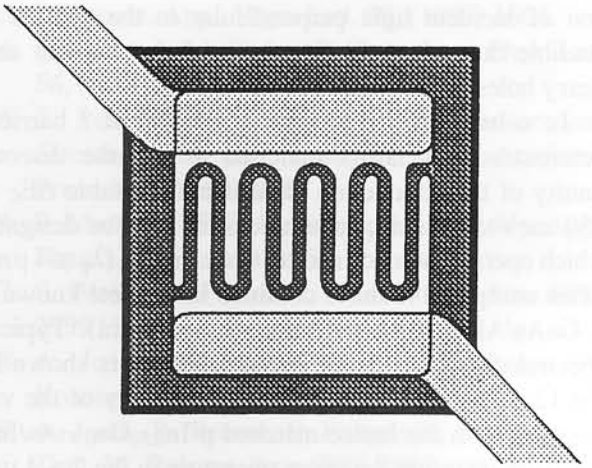

Fig. 9. InGaAs/InAlAs photodiode with polyamide insulation, fabricated in IET.

5. Metal – semiconductor – metal detectors

Metal-semiconductor-metal photodiodes (MSM PD) consist of a semiconductor layer which absorbs radiation, and two interdigitated metal electrodes deposited on top of it to form back-to-back Schottky diodes. Since the structures are planar, the capacitance is particularly low when the semiconductor layer is depleted due to the applied bias. Therefore, this detectors are fast and have very low noise, which is indispensable in the case of optoelectronic integrated circuits. The advantages of these diodes were often demonstrated in the case of detection of $\lambda \cong 0.8$ μm radiation. Van Zeghbroeck et al. [13] fabricated MSM PD on GaAs with a record cut-off frequency of 105 GHz. Nevertheless, $In_xGa_{1-x}As$ detectors of (1.3 ÷ 1.55) μm radiation are still extensively investigated. This is due to the fact that the dark current in $In_xGa_{1-x}As$ MSM PD is relatively high because of the small height of Schottky barrier (≅ 0.2 eV) in this structure. Growing an additional layer of InAlAs is the most promising method to heighten the barrier [14]. Wide-bandgap $In_xAl_{1-x}As$ (x = 0.52) lattice-matched to $In_xGa_{1-x}As$ (x = 0.53) grown on InP has a high Schottky barrier. A thin layer of InAlAs (≅ 60 nm) heightens the barrier both for electrons (up to ≅ 0.8 eV) and holes. Using these heterostructures (see Fig. 9) cut-off frequencies of 6.2 GHz were obtained [15].

A substantial progress in reduction of dark current was achieved recently due to a deposition of additional layers of CdS (7 nm) [16], Si_3N_4 (200 nm) [17], or metallic barrier engineering [18]. Dark currents with record low values of 0.13 and 0.44 pA/μm² were obtained with the bias of 5 V and 10 V, respectively [18].

Alternative designs of a MSM $In_xGa_{1-x}As$ detector grown on GaAs and operating in the same spectral region were reported. One such structure fabricated by means of MBE at a relatively low temperature is shown in Fig.10. The active layer of the detector consists of a strained superlattice: 120 periods of 6 nm GaAs and 6 ÷ 8 nm $In_{0.66}Ga_{0.34}As$. The total thickness of the active superlattice is several times higher than the critical one. Nevertheless, it is widely known that a thick, strained superlattice consisting of thin films, with the thickness of each film lower than the critical one, relaxes as a whole, therefore, misfit dislocations are located at the superlattice/substrate interface. Moreover, the superlattice prevents misfit dislocations

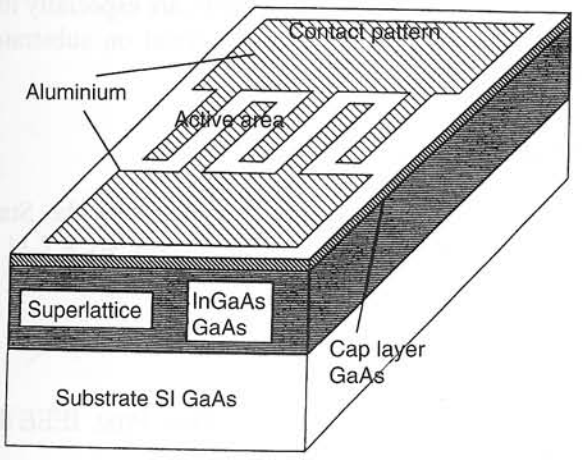

Fig. 10. MSM PD structure with a relaxed superlattice $In_xGa_{1-x}As$/GaAs on GaAs substrate [19].

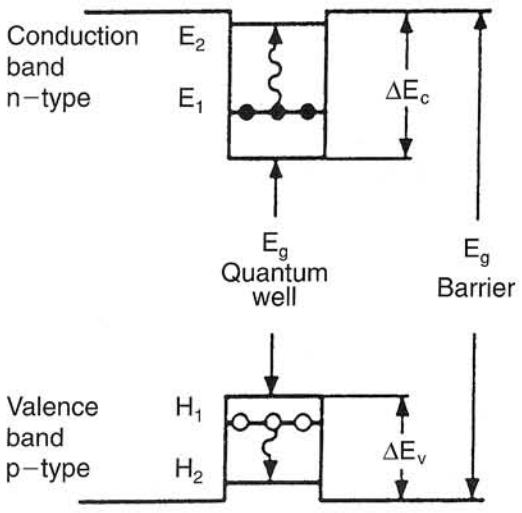

Fig. 11. Band diagram of a quantum well with depths ΔE_C and band ΔE_V. Intraband absorption for electron transitions from E_1 to E_2 or hole transitions from H_1 to H_2 is marked schematically.

from propagating to the active region of the diode. If this structure is fabricated using MBE it is possible to fabricate near-ideal *in situ* Al barriers on the surface of GaAs [20].

6. Quantum – well infrared photodetectors

Interband optical absorption involves transitions between the conduction and valence bands. This leads to generation of free carriers – both electrons and holes. The photocarriers are collected in the detector structure and thus a photocurrent is produced.

Intraband (intersubband) transitions between discrete levels in quantum wells may also be used to detect radiation. These transitions are marked schematically in Fig.11. The carriers may pass the potential barrier even if $h\nu < E_g$. Thus the mechanism of absorption is related to the excitation of electron (hole) from the ground state in a doped well to an excited state in the same band. The wells of quantum detectors are designed in such a way that the excited carrier may escape and contribute to the photocurrent.

An important advantage of quantum detectors is the fact that their spectral characteristics may be shaped through the choice of material and the thickness of quantum wells. In the case of n-type doped wells the quantum-mechanical selection rules in point of the conduction band forbid electron transitions with the incident light perpendicular to the surface. Therefore, these structures must be illuminated usually at an incidence angle of 45°. On the other hand, in p-type doped wells absorption of incident light perpendicular to the surface is possible due to strong interactions between light and heavy holes in the valence band for $k \neq 0$.

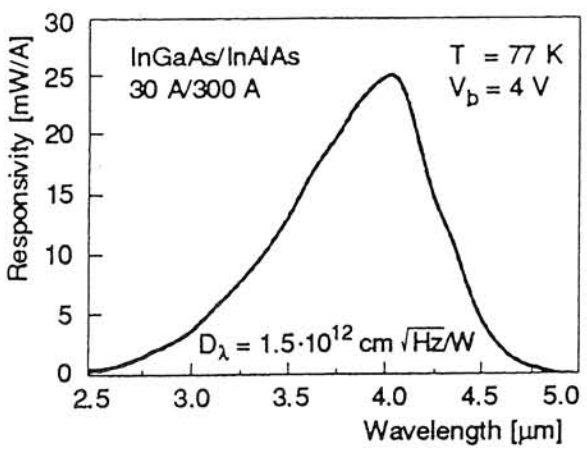

Fig. 12. Spectral characteristic of a quantum-well infrared photodetector $In_{0.53}Ga_{0.47}As$ / $In_{0.52}Al_{0.48}As$ on InP at T = 77K [21].

In n-$In_{0.53}Ga_{0.47}As$/$In_{0.52}Al_{0.48}As$ (well / barrier) heterostructures lattice-matched to InP the discontinuity of the conduction band is considerable ΔE_C = 550 meV). Thus a quantum detector may be designed which operates at much shorter wavelengths ($\lambda_p \cong 4$ μm) when compared to those obtained in the best known n – GaAs/$Al_xGa_{1-x}As$ detectors (6 ÷ 18 μm). Typical spectral characteristic of such a detector is shown in Fig.12. Due to a considerable discontinuity of the valence band in the lattice-matched p-$In_{0.53}Ga_{0.47}As$/InP structure quantum detectors operating in the 2 ÷ 4 μm range with λ_p = 2.7 μm were obtained.

Since many combinations of well and barrier materials are possible, we will only mention the already fabricated quantum detectors containing $In_xGa_{1-x}As$.

n-$In_{0.53}Ga_{0.47}As$/ /$In_{0.52}Al_{0.48}As$	$\lambda_p \cong 4$ μm	lattice-matched [21]
n-$In_{0.53}Ga_{0.47}As$/InP	$\lambda_p \cong 8$ μm	lattice-matched [22]
n-$In_{0.15}Ga_{0.85}As$/GaAs	$\lambda_p \cong 15$ μm	strained well [23]
p-$In_{0.53}Ga_{0.47}As$/InP	$\lambda_p \cong 2.7$ μm	lattice-matched [24]
p-$In_{0.53}Ga_{0.47}As$/InP	$\lambda_p \cong 6.7$ and 10.9 μm	(higher orders) lattice-matched [25]

7. Summary

The results of research, both theoretical and experimental, conducted so far indicate that $In_xGa_{1-x}As$ is a perfect material for optoelectronic devices – sources, modulators and detectors of radiation. These devices may be optimized to operate at any given wavelength between the long-wave edge of the visible range and approximately 3.5 μm. This range may be extended through bandgap engineering. Low-temperature epitaxy methods, particularly MBE, are especially important for deposition of this material on substrates with a different lattice constant.

Acknowledgment

This work was partially supported by the State Committee for Scientific Research grant No. 8 T 11 B 037 11.

References

1. H. Morkoc, B. Sverdlov, G. Gao, Proc. IEEE **81**, (1993) 493.
2. G. Huang, U. Reddy,T. Henderson, R. Haudre, H. Morkoc, J. Appl. Phys. **62**, (1987) 3366.

3. R. People, Appl. Phys. Lett. **50**, (1987) 1604.
4. S. Gutha, A. Madhukar, L.Chen, Appl. Phys. Lett. **56**, (1990) 2304.
5. T. Pearsall, M. Pollack, *Semiconductors and Semimetals* 22, ch.2 ; ed by W.Tsang, Academic Press, New York 1985.
6. R. Martinelli, T. Zamerowski, P. Longeway, Appl. Phys. Lett. **53**, (1988) 989.
7. S. Wojtczuk, P. Colter, M. Jhabvala, Proc SPIE **2999** (1997) – to be published.
8. A. Joshi, V.Ban, S. Mason, M. Lange, W. Kosonocki, Proc. SPIE **1735**, (1992) 287.
9. A. Joshi, R. Brown, E. Fitzgerald, X. Wang, S. Ting, M. Bulsara, Proc SPIE **2999** (1997) – to be published.
10. J. Piotrowski, W. Galus and M. Grudzień, Infrared Phys. **31**, (1991) 1.
11. F. Capasso; *Heterojunction band discontinuities* ed. by F. Capasso, and G Margeritondo, North-Holland, p. 429 (1987).
12. T. Kagawa, Y. Kawamura, H. Asai, M. Naganuma, Appl. Phys. Lett. **57**, (1990) 1895.
13. J. Van Zeghbroeck, Ch. Harder, P. Wolf, Tech. Dig. IEDM, Washington DC, p. 279 (1987).
14. J. Soole, H. Schumacher, IEEE J. Quantum Electron. **27**, (1991) 737.
15. P. Nytkens, J. del Alamo, MIT Annual Report p. 113 (1994).
16. K. Vaccaro, A. Davis, S. Spaziano E. Martin, I. Lorentzo, J. Electron. Mat. **25**, (1996) 603.
17. W. Wohlmuth, M. Arafa, A. Mahajan, P. Fay, I. Adesida, Appl. Phys. Lett. **69**, (1996) 3578.
18. W. Wohlmuth, P. Fay, C. Caneanu, I. Adesida, Electron. Lett. **32**, (1996) 249.
19. M. Zirngibl, M. Ilegems, J. Appl. Phys. **69**, (1991) 8392.
20. M. Kaniewska, K. Regiński, J. Kaniewski, L. Ornoch, M. Bugajski, Acta Phys. Pol. **88**, (1995) 775.
21. G. Hasnain, B. Levine, D. Sivco, A. Cho, Appl. Phys. Lett. **56**, (1990) 770.
22. S. Gunapala, B. Levine, D. Ritter, R. Hamm, M. Panish, Appl. Phys. Lett. **58**, (1991) 2024.
23. B. Levine, J. Appl. Phys. **74**, (1993) R1.
24. S. Gunapala, B. Levine, D. Ritter, R. Hamm, M. Panish, J. Appl. Phys. **71**, (1992) 2458.
25. J. Katz, Y. Zhang, W. Wang, Electron. Lett. **28**, (1992) 932.